# Toxicology Research

Accepted Manuscript






ROYAL SOCIETY OF CHEMISTRY

www.rsc.org/toxicology

# Cumulative metabolic effects of low-dose benzo(a)pyrene exposure on human cells

Qian Ba[1,2,#], Chao Huang[1,#], Yijing Fu[1], Junyang Li[1], Jingquan Li[1,2], Ruiai Chu[1,2], Xudong Jia[2,*], Hui Wang[1,2,3,*]

[1]*Key Laboratory of Food Safety Research, Institute for Nutritional Sciences, Shanghai Institutes for Biological Sciences, Chinese Academy of Sciences, Shanghai, China;*

[2]*Key Laboratory of Food Safety Risk Assessment, Ministry of Health, Beijing, China;*

[3]*School of Life Science and Technology, ShanghaiTech University, Shanghai, China.*

[#]These authors contributed equally to this work.

[*]Correspondence to: Hui Wang, Institute for Nutritional Sciences, Shanghai Institutes for Biological Sciences, Chinese Academy of Sciences, Rm 2204, Newlife Building A, 320 Yueyang Rd, Shanghai 200031, China, E-mail: huiwang@sibs.ac.cn, or Xudong Jia, Key Laboratory of Food Safety Risk Assessment, Ministry of Health, Beijing 100021, China, E-mail: jiaxudong@cfsa.net.cn.

## Abstract

Benzo(a)pyrene (B[a]P) is a common environmental and foodborne pollutant which has been identified as the Group I carcinogen. Although the carcinogenicity of B[a]P has been illustrated, its comprehensive influences on metabolism and the further relevance in adverse health outcome are not well understood. To investigate the global metabolic effects of long-term B[a]P exposure at environmental dosage, we utilized the human SMMC-7721 cells-based B[a]P exposure models to perform the metabolomics study and network analysis. A total of 316 biochemicals were identified and 104 metabolites were found to be significantly altered. Bioinformatics analysis showed that the amino acid, carbohydrate, lipid metabolism pathway and nucleotide metabolism pathway were influenced by prolonged B[a]P exposure. Notably, the metabolic effects of B[a]P varied with different dosages. In addition, B[a]P exposure declined the glycolysis process but enhanced the glycolytic capability of SMMC-7721 cells *in vitro*. These findings establish the overall B[a]P-induced metabolic network, characterize the metabolic effects of chronic and environmental B[a]P exposure on human-relevant cells, and enhance the understanding of the adverse outcome pathway frame of B[a]P.


**Keywords:** Benzo(a)pyrene, metabolomics, network analysis, glycolysis, glycolytic capability, human metabolism.

## Introduction

Benzo(a)pyrene (B[a]P), a prototypical member of the polycyclic aromatic hydrocarbons (PAHs) [1, 2], is formed in the process of incomplete combustion of organic materials [3, 4]. B[a]P has been listed as the Group 1 carcinogen by the International Agency for Research on Cancer (IARC) [5]. As a typical environmental and foodborne pollutant, B[a]P exposure is almost inevitable for human through the ingestion of charcoal-grilled foods and contaminated water, the inhalation of engine exhaust fumes and cigarette smoke [6, 7]. Therefore, it is important to reveal the cumulative toxicity and the molecular effects of B[a]P in the environment thoroughly.

Once taken up into cells, B[a]P is metabolized to form various reactive metabolites, which elicit toxicity through binding covalently to cellular elements such as DNA and generating reactive oxygen species to damage cellular macromolecules [8, 9]. However, although the toxic effects of B[a]P including teratogenicity, carcinogenicity, neurotoxicity, immunotoxicity, etc., have been studied [10-13], most understanding of the bio-safety assessment of B[a]P has been obtained from the high-dose toxicity evaluation with laboratory animals, which is not conclusive to illustrate the effects of prolonged B[a]P exposure at lower environmental concentrations. It is recommended by the U.S. National Research Council to transform the toxicity testing from high-dose animal studies to pathway–based approaches using human-relevant cells [14, 15]. We have established a long-term and low-dose B[a]P exposure model based on human SMMC-7721 cells [16], which provides a useful tool to explore the cumulative

toxicity of low-dose B[a]P on human cells.

To achieve a comprehensive understanding of the toxicological behavior of B[a]P, it is necessary to analyze the global molecular responses in the cells. Among them, metabolic perturbation, which usually manifests as metabolite profiling changes, is a common event in pollutant-induced toxicity. In the adverse outcome pathway (AOP) frame, metabolism perturbation represents a typical key event (KE) which originates from the molecular initiating events (MIE) such as gene/protein expression changes and subsequently induces cell phenotypic effects. And metabolomics is capable of providing the global metabolic status and the whole-cell response [17], which makes it a reasonable and effective technique to determine the metabolic profiles induced by B[a]P exposure. However, although some studies about the metabolic effects of B[a]P in animals, including fish, earthworms and rats, have been reported [18-20], the potential influence of prolonged B[a]P exposure, especially at lower environmental doses, on metabolic disruption of human cells are rarely reported.

In this study, we investigated the chronic toxicological effects of B[a]P on the global metabolic profiling in the human cells with long-term and low-dose B[a]P exposure. The metabolites significantly altered were identified using the gas chromatography/mass spectrometry (GC/MS) and liquid chromatography/mass spectrometry (LC/MS/MS) based approaches. And the potential altered metabolic process and pathways were explored through bioinformatics analyses. This study

characterizes the metabolic effects of chronic and environmental B[a]P exposure on human SMMC-7721 cells and contributes to the more comprehensive understanding of the toxicity of B[a]P.

## Materials and Methods

### Cell cultures

SMMC-7721 cells originally from the Cell Bank of the Shanghai Institutes for Biological Sciences, Chinese Academy of Sciences (SIBS, CAS) were cultured in RPMI 1640 medium supplemented with 10% fetal bovine serum, 100 μg/mL penicillin, and 100 μg/mL streptomycin and maintained in an incubator with a humidified atmosphere of 5% $CO_2$ at 37°C. The cells were co-cultured by B[a]P (0.01 nM, 1 nM, 100 nM) or 0.1% DMSO for a month and subjected to the subsequent analyses as described previously [16].

### Metabolomics analysis

Cells were washed with 10 mL of PBS, trypsinized with 0.25% Trypsin-EDTA, and washed ice-cold PBS. About $9\times10^6$ cells from each triplicate sample were pelleted, flash frozen in liquid nitrogen, and stored at -80°C. Cell pellets were shipped to Metabolon, Inc. (SJTU-Metabolom Joint Metabolomics Laboratory), on dry ice for metabolomics analysis. At the time of analysis, samples were extracted and split into equal parts for analysis by GC/MS and LC/MS/MS platforms [21, 22]. Several technical replicate samples created from a homogeneous pool containing a small amount of all

study samples were also included. Global biochemical profiles, from DMSO-treated SMMC-7721 cells and cells treated for one month with varying doses of B[a]P (0.01 nM, 1 nM, 100 nM) were compared.

The LC/MS portion of the platform was based on a Waters ACQUITY UPLC (Waters, Milford, MA) and a Thermo-Finnigan LTQ mass spectrometer (Thermo Electron Corporation, San Jose, CA), which consisted of an electrospray ionization source and linear ion-trap mass analyzer. The sample extract was split into two aliquots, dried, then reconstituted in acidic or basic LC-compatible solvents, each of which contained 11 or more injection standards at fixed concentrations. One aliquot was analyzed using acidic positive ion-optimized conditions and the other using basic negative ion-optimized conditions in two independent injections using separate UPLC columns (Waters UPLC BEH C18-2.1 x 100 mm, 1.7 μm). Extracts reconstituted in acidic conditions were gradient-eluted using water and 95% methanol, both containing 0.1% formic acid, while the basic extracts were gradient-eluted with water and 95% methanol contained 6.5 mM ammonium bicarbonate. The MS instrument scanned 99-1000 m/z and alternated between MS and MS2 scans using dynamic exclusion with approximately 6 scans per second.

The samples destined for GC/MS analysis were re-dried under vacuum desiccation for > 24 h prior to being derivatized under dried nitrogen using bistrimethyl-silyl-triflouroacetamide (BSTFA). The GC column was 5% phenyl

dimethyl silicone column with helium as the carrier gas and the temperature ramp is from 40 to 300°C in a 16 min period. Samples were analyzed on a Thermo-Finnigan Trace DSQ fast-scanning single-quadrupole mass spectrometer operated at unit mass resolving power with electron impact ionization and a 50-750 atomic mass unit scan range. The information output from the raw data files was automatically extracted.

Metabolites were identified by automated comparison of the ion features in the experimental samples to a reference library of chemical standard entries that included retention time, molecular weight (m/z), preferred adducts, and in-source fragments as well as their associated MS/MS2 spectra. This library allowed the rapid identification of metabolites in the experimental samples with high-confidence.

**Network construction and analysis**

Cytoscape software (Version 3.1.1; http://www.cytoscape.org) and the MetScape plugin (Version 3.0.2) were used to construct the Compound-Reaction-Enzyme-Gene (CREG) metabolic network. The enriched pathways of metabolic network were from an internal relational database stored at NCIBI which integrates data from Kyoto Encyclopedia of Genes and Genomes (KEGG) and Edinburgh Human Metabolic Network (EHMN). With the plugin BiNGO (Version 3.0.2) in Cytoscape, the Gene Ontology (GO) terms that statistically overrepresented are obtained from the genes in the CREG metabolic network.

153 **Metabolic flux analysis**

154 The glycolytic flux of SMMC-7721 cells was determined by directly measuring the
155 extracellular acidification rate (ECAR) using an XF24 extracellular flux analyzer
156 (Seahorse Bioscience, MA, USA). DMSO- or B[a]P-treated cells were seeded in the
157 XF24 microplate at a density of 35,000 cells per well and incubated overnight. On the
158 day of metabolic flux analysis, the culture medium was replaced with XF Glycolysis
159 Stress Test Assay Medium and incubated at 37°C in a non-$CO_2$ incubator for 1 hr. The
160 cells were immediately analyzed in the Seahorse XF24 Extracellular Flux Analyzer
161 following injection of compounds: glucose (10 mM), oligomycin (1 μM), and 2-DG
162 (50 mM). ECAR were calculated by the Seahorse XF-24 software. Data are presented
163 as Mean ± SD.

164

165 **Statistical analysis**

166 For metabolomics results, Welch's two-sample *t*-test was used to identify
167 biochemicals that differed significantly between B[a]P treatment and control groups.
168 Differences between groups were considered significant ($p \leq 0.05$) or approaching
169 significant ($0.05 < p < 0.10$). For metabolic flux results, Student's *t*-test was used to
170 examine the statistical significance of differences. $p < 0.05$ was considered statistically
171 significant.

172

173 **Results**

174 **Metabolomics analysis**

We have established a low-dose and long-term B[a]P-exposed model based on human SMMC-7721 cell lines, which are capable to metabolically activate B[a]P [16]. To explore the environmental-relevant toxicity, we used a range of concentrations, which are comparable to the serum B[a]P levels of populations exposed environmentally (≤ 3.88 ± 2.22 nM) [23], and a continuous exposure for 1 month. To investigate the metabolic effects of B[a]P on SMMC-7721 cells, DMSO and B[a]P-treated SMMC-7721 cells were collected for metabolomics analysis by GC/MS and LC/MS/MS. Overall, a total of 316 biochemicals were identified (Table S1). Of which, 22 ($p \leq 0.05$) or 28 ($0.05 < p < 0.10$) compounds in 0.01 nM groups, 27 ($p \leq 0.05$) or 22 ($0.05 < p < 0.10$) compounds in 1 nM groups, and 21 ($p \leq 0.05$) or 22 ($0.05 < p < 0.10$) compounds in 100 nM groups were significantly altered by B[a]P exposure compared with control groups. In 0.01 and 100 nM groups, most of the significant altered biochemicals were increased, while in 1 nM groups, B[a]P induced the reduced biochemicals almost as many as the increased biochemicals (Table 1).

**Network analysis**

In order to mining more useful information and eliminate the noise signal, the bioinformatics approaches were performed to predict the metabolic pathways [24]. After the exclusion of repeated entries, 104 altered compounds ($p < 0.1$) were identified, and 70 of them could be mapped to KEGG IDs (Table S2), which were used to create a Compound-Reaction-Enzyme-Gene (CREG) metabolic network through the Metscape software [25]. The CREG graph gives an overview of all components of

B[a]P-induced metabolic network. By integrating the metabolites, reactions, enzymes and genes, the CREG network could provide comprehensive information about B[a]P-induced metabolic responses. Among them, the potential B[a]P-altered genes in the network were shown in Table S3. In our CREG network, the largest two subnetworks occupy 86% of the full network and contain most differential metabolites (Figure S1). The experimental differential metabolites and related metabolic pathways in the two major subnetworks were marked in Figure 1. To determine the overrepresented Gene Ontology (GO) categories in B[a]P-induced metabolic network, we used the BiNGO plugin [26] to map the predominant functional themes from the genes in CREG network and visualize them as a Cytoscape graph. The major functional superpathways of GO terms were amino acid, carbohydrate, lipid metabolism pathway and nucleotide metabolism pathway (Figure 2), suggesting that these metabolic processes were influenced significantly by B[a]P.

**Nucleotide metabolism**

The catabolism of purine especially adenosine was enhanced after B[a]P treatment, as the end product of purine breakdown, urate, was accumulated, and the levels of intermediates, such as adenine, hypoxanthine and xanthine, were diminished (Figure 3A). However, B[a]P treatment elevated the levels of inosine 5'-monophosphate (IMP) at the dosage of 100 nM (Figure 3A), which is the first nucleotide formed in purine *de novo* synthesis and indicated that 100 nM of B[a]P enhanced the activity of purine anabolism. Consistently, the levels of purine biosynthesis intermediates, including

adenylosuccinate, adenosine 5'-monophosphate (AMP), adenosine 5'-diphosphate (ADP) and guanosine 5'-monophosphate (5'-GMP) showed higher levels in 100 nM B[a]P-treated groups (Figure 3A). The enhanced purine anabolism also resulted in the increase of adenosine and inosine (Figure 3A).

In the 0.01 and 1 nM groups, the contents of uracil anabolites (carbamoylasparate, orotate) were reduced (Figure 3B), and the catabolites of uracil, (dihydrouracil, β-alanine) were increased (Figure 3B), suggesting that B[a]P treatment inhibited uracil anabolism and promoted uracil catabolism at 0.01 and 1 nM. Also, the level of uracil was reduced in 0.01 and 1 nM B[a]P-treated groups (Figure 3B), which was partially due to the decreased anabolism and enhanced catabolism, but also because of the increased transformation of uracil to uridine (Figure 3B). However, with the increase of concentration, the anabolism of uracil enhanced and the catabolism weakened gradually. B[a]P treatment at 100 nM results in elevated levels of carbamoylasparate and orotate (Figure 3B). Simultaneously, dihydrouracil and β-alanine were decreased compared to those in 0.01 and 1 nM treatment groups (Figure 3B). Overall, B[a]P promoted the synthesis of uridine and uridine monophosphate (UMP) (Figure 3B).

**Carbohydrate and energy metabolism**

SMMC-7721 cells exposed to 0.01 and 1 nM of B[a]P exhibited reduced glucose and elevated sorbitol and fructose levels compared to vehicle controls (Figure 4A), which

may suggest a change in glucose uptake and/or utilization. Notably, 0.01 nM of B[a]P resulted in a modest accumulation of the glycolytic intermediates 3-phosphoglycerate and phosphoenolpyruvate (PEP) as well as the end products pyruvate and lactate (Figure 4B). However, PEP and pyruvate levels were diminished in 1 and 100 nM B[a]P-treated groups, potentially suggesting a concentration-dependent decrease in glycolytic metabolism (Figure 4B). Besides, B[a]P treatment at the 1 nM dosage resulted in lower levels of multiple pentose phosphate pathway metabolites including 6-phosphogluconate, pentulose 5-phosphates, and ribose 5–phosphate (Figure 4C).

Aside from glucose metabolism, B[a]P treatment promoted a selective accumulation of the TCA cycle intermediates citrate and cis-aconitate. In contrast, α-ketoglutarate (α-KG), fumarate, and malate were modestly reduced at 1 nM, but not 0.01 or 100 nM dosages (Figure 4D). Higher levels of citrate may promote lipogenesis. Similarly, elevated coenzyme A and pantothenate levels (Figure 4E) may also impact mitochondrial metabolism as coenzyme A participates in oxidative metabolism. Altogether, these findings may suggest that B[a]P have significant effects on carbohydrate and energy metabolism.

**Arginine metabolism**

Compared to vehicle controls, B[a]P-exposed cells exhibited an accumulation of dimethylarginine (Figure 5A), which is produced from the degradation of methyl arginine containing proteins. Accordingly, multiple peptides such as

phenylalanylglutamate and leucylglycine were elevated (Figure 5A). These results may reflect a change in proteolytic processing and/or protein synthesis. 0.01 and 1 nM B[a]P also induced high levels of creatinine and creatine (Figure 5A), which are synthesized from glycine, arginine, and methionine, thus may reflect a change of the arginine utilization to creatine. Consistently, another arginine-related metabolite, ornithine, was diminished in response to B[a]P treatment (Figure 5A). These changes may consequently restrict the availability of polyamines synthesis (putrescine and spermidine), as suggested by decreased levels of the synthetic by-product, 5-methylthioadenosine (MTA) (Figure 5A).

**Branched chain amino acid metabolism**

Although levels of the branched chain amino acids (BCAA) valine, isoleucine, and leucine were similar between different groups (data not shown), 100 nM of B[a]P selectively induced the α-keto acids analogue (3-methyl-2-oxovalerate and 4-methyl-2-oxopentanoate) (Figure 5B), suggesting a potential disruption in BCAA catabolism. Consistently with this, 100 nM of B[a]P treatment resulted in lower levels of the downstream catabolites (isovalerylcarnitine, isobutyrylcarnitine, and 2-methylbutyrylcarnitine) and the end product (propionylcarnitine) compared to 0.01 and 1 nM B[a]P-treated cells (Figure 5B). Thus, B[a]P may induce the disruption of BCAA catabolism at 100 nM dosage.

**Glycolysis rate**

To confirm that the decrease in glucose uptake/utilization in the B[a]P-exposed cells correspond with a decreased rate of glycolysis, the extracellular acidification rate (ECAR), a surrogate of glycolysis, was measured using a Seahorse XF24 extracellular flux analyzer. The basal ECAR significantly decreased after B[a]P treatment (Figure 6A), indicating that the glycolysis rate decreased in SMMC-7721 cells after B[a]P exposure. However, after injection of oligomycin, an ATP synthase inhibitor, which shifts the energy production to glycolysis and reveals the cellular maximum glycolytic capacity, the increases of ECAR in B[a]P-exposed SMMC-7721 cells were more sharply than that in control group (Figure 6B). These results suggest that long-term B[a]P exposure could confer SMMC-7721 cells more robust glycolytic capability, which may benefit the cells under harsh conditions *in vivo*.

## Discussion

In this study, we investigated the potential metabolic effects of long-term B[a]P exposure at environmental doses on human-relevant cells SMMC-7721. Metabolomics study and bioinformatics analysis showed that prolonged B[a]P exposure could cause metabolic perturbation in amino acid, carbohydrate, lipid metabolism pathway and nucleotide metabolism pathway. Metabolic flux analysis also showed the influence of B[a]P exposure on glycolysis and the glycolytic capability. Overall, we characterized B[a]P-induced cumulative metabolic effects on SMMC-7721 cells.

Systems biology provides a powerful approach to discover the molecular perturbations of environmental pollutants on biological systems. And the metabolism perturbation usually represents the sensitive and common events in pollutant-induced toxicity. Moreover, the metabolic toxicity always plays as the KE to link MIE (gene/protein expression) and the specific adverse outcome (phenotype), thus it is important to depict the metabolic effects of environmental pollutants for the AOP network. Although the carcinogenic and mutagenic toxicity of B[a]P have been studied, the metabolic effects of B[a]P, especially the prolonged exposure at environmental dose, are still not well understood. To characterize the metabolic toxicity of B[a]P, we used a range of doses comparable to the serum B[a]P levels of populations exposed environmentally [23] and continuously treated for 1 month to assess the cumulative toxicological effects.

It is known that B[a]P could form DNA adducts through its metabolite, 7,8-dihydroxy-9,10-epoxy-7,8,9,10-tetrahydrobenzo[a]pyrene (BPDE) [27]. However, we found that the prolonged B[a]P exposure could altered the nucleotide metabolism even at the low dosages. This metabolic effects of B[a]P varied with different dosages. Within the concentration range of 0.01 and 100 nM, B[a]P tends to induce stronger activity of nucleotide catabolism in lower dose, and nucleotide anabolism is likely to be enhanced by higher dose of B[a]P exposure. How these alterations affect the cumulative effects of B[a]P on SMMC-7721 cells need further investigation. Overall, the ultimate levels of nucleotide (AMP, GMP, UMP, and CMP) were increased

329 gradually with the concentrations of B[a]P, which may be the cellular adaptive
330 responses to overcome the BPDE-DNA adducts-induced DNA replication stress and
331 damage. This process may lead to errors in DNA replication and introduce gene
332 mutations, thus increase the risk of cancer.
333
334 In addition to DNA damage, the process of B[a]P metabolism also generates reactive
335 oxygen species (ROS) and causes oxidative damage in cells [9]. Consistently, in our
336 study, B[a]P treatment elevated the levels of oxidized glutathione (GSSG), which
337 indicates that B[a]P induced a disruption of redox homeostasis and oxidative stress in
338 cells. Furthermore, B[a]P-treated cells also exhibited higher levels of the lipid
339 peroxidation products (13-HODE and 9-HODE) (Table S1), thus confirmed the lipid
340 oxidative damage induced by B[a]P. Continued oxidative stress can damage a variety
341 of organelles and macromolecules, lead to chronic inflammation, and represents an
342 important cancer risk factor.
343
344 The reprogramming energy metabolism is another hallmark of cancer [28]. In our study,
345 both the metabolomics analysis and metabolic flux detection indicated that prolonged
346 B[a]P exposure decreased the glycolysis rate in SMMC-7721 cells. Interestingly,
347 B[a]P conferred SMMC-7721 cells more robust glycolytic capability. These results
348 may suggest that long-term B[a]P exposure makes cancer cells more adaptable to a
349 wide variety of environments. In culture condition *in vitro*, which is a sufficient
350 oxygen environment, B[a]P-treated cells show low level of glycolytic activity, and use

more efficient aerobic respiration. However, under some harsh conditions *in vivo* especially in the oxygen-deficient environment, B[a]P-treated cancer cells, which have accessed the higher glycolytic capacity, could switch to elevated glycolysis and acquire adequate energy. This is consistent with our previous report that B[a]P promoted cancer aggressiveness and progression of SMMC-7721 cells [16].

## Conclusions

In summary, we have established the overall B[a]P-induced metabolic network, revealed the global influences of long-term and low-dose B[a]P exposure on metabolism in SMMC-7721 cell, and identified the major altered pathways including amino acid, carbohydrate, lipid metabolism pathway and nucleotide metabolism pathway. These metabolic alterations may further contribute to cancer deterioration and is potential to explore more sensitive biomarkers for early detection of B[a]P toxicity, thus contributes to more comprehensive understanding of the toxicity of B[a]P.

## Conflict of Interests

The authors declare that they have no conflict of interest.

## Acknowledgements

This work was supported by grants from the National Natural Science Foundation of China (31200569 and 81125020), the Ministry of Science and Technology of China

(2012CB720804), the Key Research Program (KSZD-EW-Z-021 and KSZD-EW-Z-019) and the Instrument Developing Project of the Chinese Academy of Sciences, the Science and Technology Commission of Shanghai Municipality (14391901800), and the Food Safety Research Center of INS, SIBS, CAS.

## References

1. D. H. Phillips, *Nature*, 1983, **303**, 468-472.
2. S. K. Srivastava, H. Xia, A. Pal, X. Hu, J. Guo and S. V. Singh, *Cancer letters*, 2000, **153**, 35-39.
3. H. V. Gelboin, *Physiological reviews*, 1980, **60**, 1107-1166.
4. D. Benford, M. Dinovi and R. W. Setzer, *Food and chemical toxicology : an international journal published for the British Industrial Biological Research Association*, 2010, **48 Suppl 1**, S42-48.
5. I. W. G. o. t. E. o. C. R. t. Humans, *IARC Monogr Eval Carcinog Risks Hum*, 2010, **92**, 1-853.
6. K. Srogi, *Environ Chem Lett*, 2007, **5**, 169-195.
7. D. H. Phillips, *Mutation research*, 1999, **443**, 139-147.
8. E. Rivedal and T. Sanner, *Cancer research*, 1981, **41**, 2950-2953.
9. H. Rubin, *Carcinogenesis*, 2001, **22**, 1903-1930.
10. A. P. Wolterbeek, E. J. Schoevers, A. A. Rutten and V. J. Feron, *Cancer letters*, 1995, **89**, 107-116.
11. D. R. Davila, D. L. Romero and S. W. Burchiel, *Toxicology and applied*

*pharmacology*, 1996, **139**, 333-341.

12. P. Mendola, S. G. Selevan, S. Gutter and D. Rice, *Mental retardation and developmental disabilities research reviews*, 2002, **8**, 188-197.

13. L. Min, S. He, Q. Chen, F. Peng, H. Peng and M. Xie, *Toxicology mechanisms and methods*, 2011, **21**, 374-382.

14. Y. Adeleye, M. Andersen, R. Clewell, M. Davies, M. Dent, S. Edwards, P. Fowler, S. Malcomber, B. Nicol, A. Scott, S. Scott, B. Sun, C. Westmoreland, A. White, Q. Zhang and P. L. Carmichael, *Toxicology*, 2015, **332**, 102-111.

15. S. Gibb, *Reproductive toxicology*, 2008, **25**, 136-138.

16. Q. Ba, J. Li, C. Huang, H. Qiu, J. Li, R. Chu, W. Zhang, D. Xie, Y. Wu and H. Wang, *Environmental health perspectives*, 2015, **123**, 246-254.

17. M. Viant and U. Sommer, *Metaboliomics*, 2013, **9**, 144-158.

18. T. D. Williams, H. Wu, E. M. Santos, J. Ball, I. Katsiadaki, M. M. Brown, P. Baker, F. Ortega, F. Falciani, J. A. Craft, C. R. Tyler, J. K. Chipman and M. R. Viant, *Environmental science & technology*, 2009, **43**, 6341-6348.

19. B. P. Lankadurai, D. M. Wolfe, A. J. Simpson and M. J. Simpson, *Environmental pollution (Barking, Essex : 1987)*, 2011, **159**, 2845-2851.

20. X. Wang, J. Zhang, Q. Huang, A. Alamdar, M. Tian, L. Liu and H. Shen, *Molecular bioSystems*, 2015, **11**, 753-759.

21. T. Ohta, N. Masutomi, N. Tsutsui, T. Sakairi, M. Mitchell, M. V. Milburn, J. A. Ryals, K. D. Beebe and L. Guo, *Toxicologic pathology*, 2009, **37**, 521-535.

22. A. M. Evans, C. D. DeHaven, T. Barrett, M. Mitchell and E. Milgram,

*Analytical chemistry*, 2009, **81**, 6656-6667.

23. M. S. Neal, J. Zhu and W. G. Foster, *Reproductive toxicology*, 2008, **25**, 100-106.

24. E. C. Butcher, E. L. Berg and E. J. Kunkel, *Nature biotechnology*, 2004, **22**, 1253-1259.

25. A. Karnovsky, T. Weymouth, T. Hull, V. G. Tarcea, G. Scardoni, C. Laudanna, M. A. Sartor, K. A. Stringer, H. V. Jagadish, C. Burant, B. Athey and G. S. Omenn, *Bioinformatics*, 2012, **28**, 373-380.

26. S. Maere, K. Heymans and M. Kuiper, *Bioinformatics*, 2005, **21**, 3448-3449.

27. G. Talaska, M. Jaeger, R. Reilman, T. Collins and D. Warshawsky, *Proceedings of the National Academy of Sciences of the United States of America*, 1996, **93**, 7789-7793.

28. D. Hanahan and R. A. Weinberg, *Cell*, 2011, **144**, 646-674.

433

434 **Figure legends**

435 **Figure 1.** Two major subnetworks within the full B[a]P-induced CREG metabolic
436 network were visualized in Cytoscape. The input metabolites altered significantly are
437 shown in red and the different metabolic pathways were marked by color traces.

438

439 **Figure 2.** The network of GO biological processes enriched by the genes from
440 B[a]P-induced CREG network. The node size shows the number of genes annotated
441 in each GO term and the node color represents the significance of the enrichment.
442 Two functional categories of GO terms are highly connected in the network (red
443 trace).

444

445 **Figure 3.** Effect of B[a]P on purine and pyrimidine metabolism. Levels of metabolites
446 in purine metabolism (**A**) and pyrimidine metabolism (**B**) were measured.

447

448 **Figure 4.** Effect of B[a]P on carbohydrate and energy metabolism. Levels of
449 monosaccharide and the derivative (**A**), glycolysis metabolites (**B**), multiple pentose
450 phosphate pathway metabolites (**C**), TCA cycle intermediates (**D**) and mitochondrial
451 metabolism products (**E**) were measured.

452

453 **Figure 5.** Effect of B[a]P on amino acid metabolism. Levels of metabolites in arginine
454 metabolism (**A**) and branched chain amino acid metabolism (**B**) were measured.

455

456 **Figure 6.** Effect of B[a]P on ECAR profiles in SMMC-7721 cells. (**A**) Basal ECAR in
457 cells exposed by B[a]P with different concentrations were shown. (**B**) Metabolic flux
458 of SMMC-7721 cells was determined with a Seahorse flux analyzer. Addition of the
459 glycolysis activity modulator (glucose, oligomycin, and 2-DG) was indicated.
460

461

**Table 1. B[a]P-induced metabolic changes in SMMC-7721 cells.**

| Welch's two-sample *t*-test | No. of biochemicals ($p \leq 0.05$) Total (↑\|↓) | No. of biochemicals ($0.05 < p < 0.10$) Total (↑\|↓) |
|---|---|---|
| 0.01 nM / Ctrl | 22 (18\|4) | 28 (20\|8) |
| 1 nM / Ctrl | 27 (12\|15) | 22 (12\|10) |
| 100 nM / Ctrl | 21 (21\|0) | 22 (20\|2) |

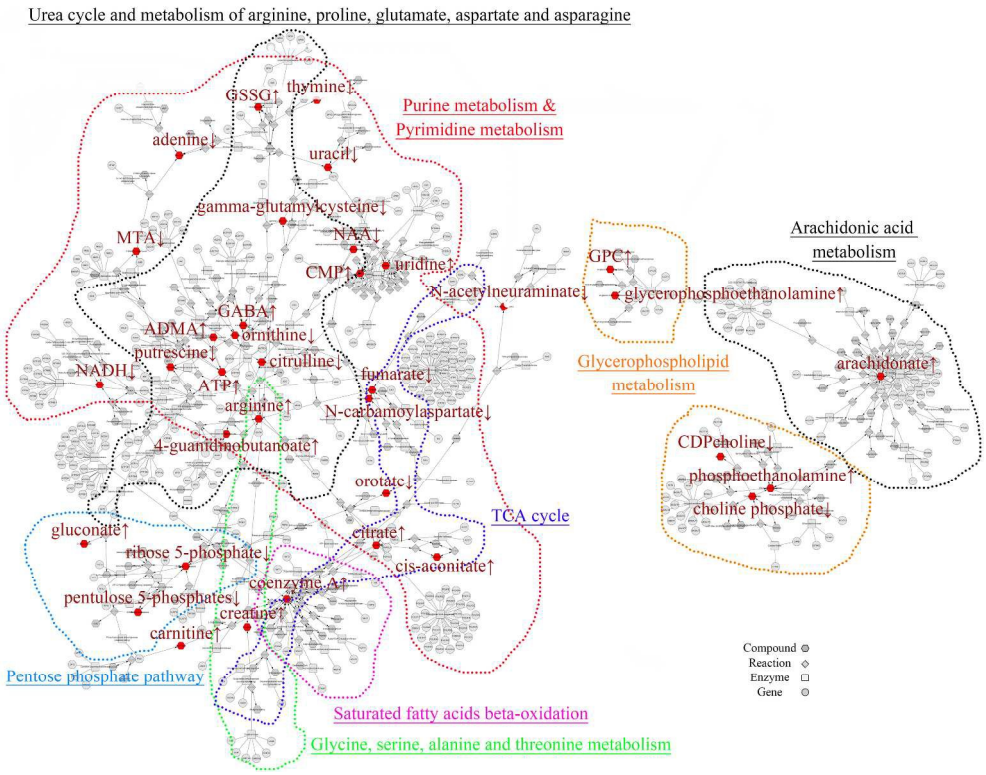


Fig 1
130x100mm (600 x 600 DPI)

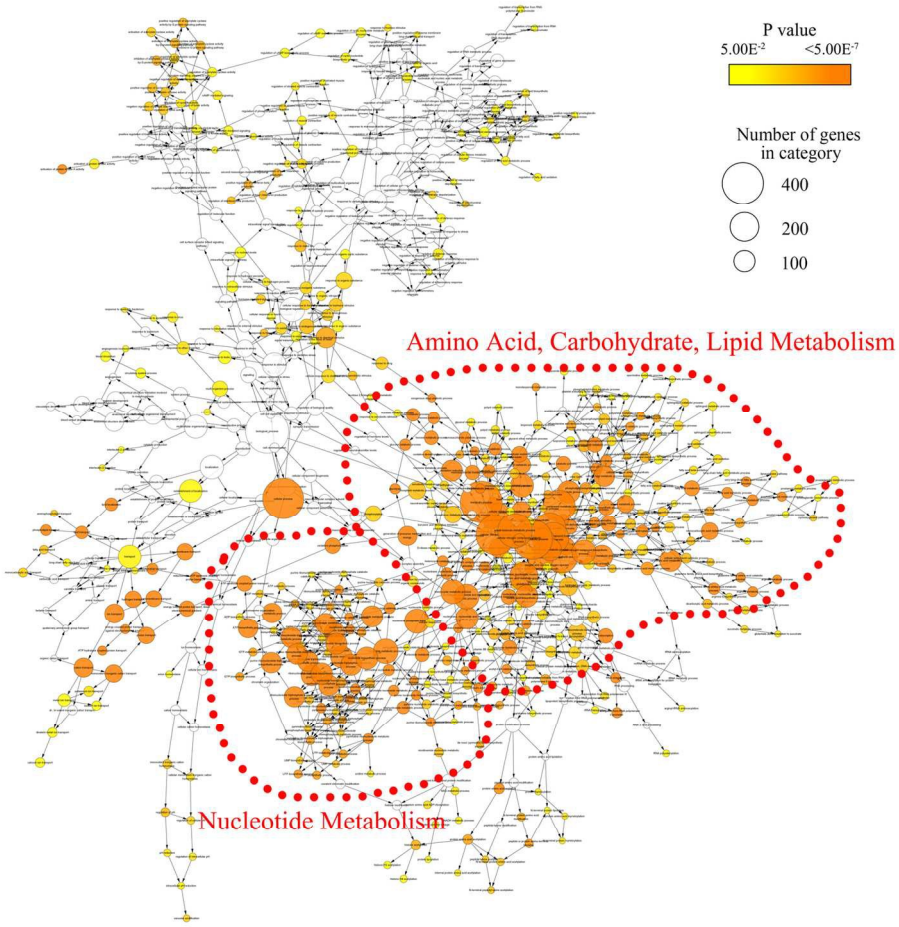


Fig 2
146x136mm (300 x 300 DPI)

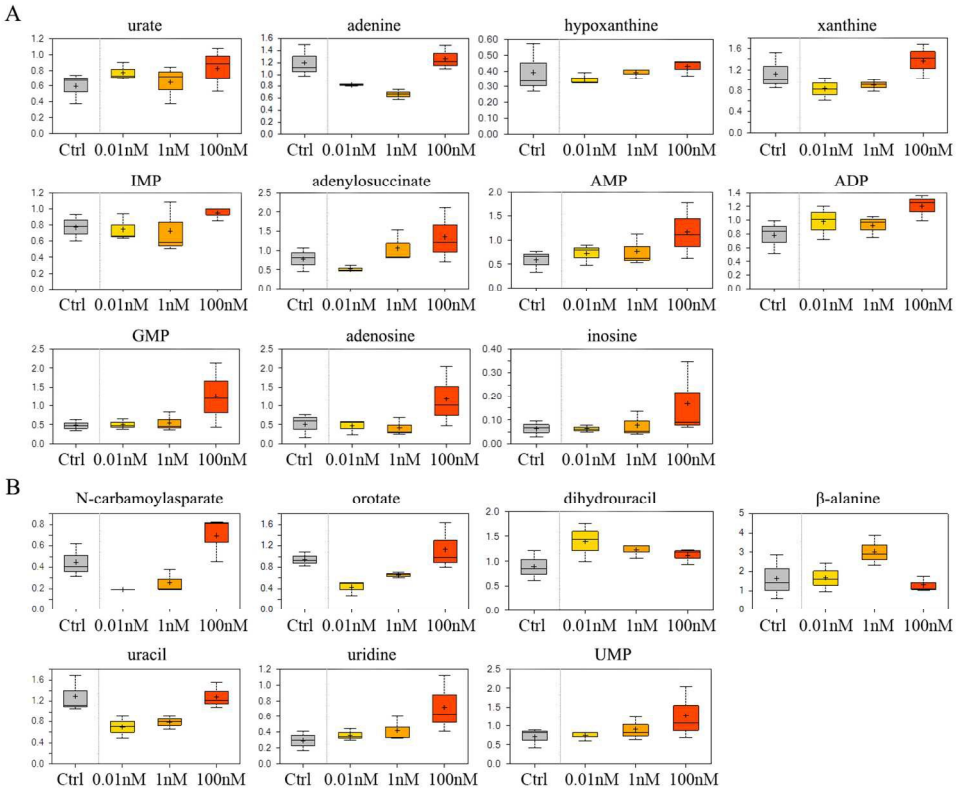


Fig 3
123x104mm (300 x 300 DPI)

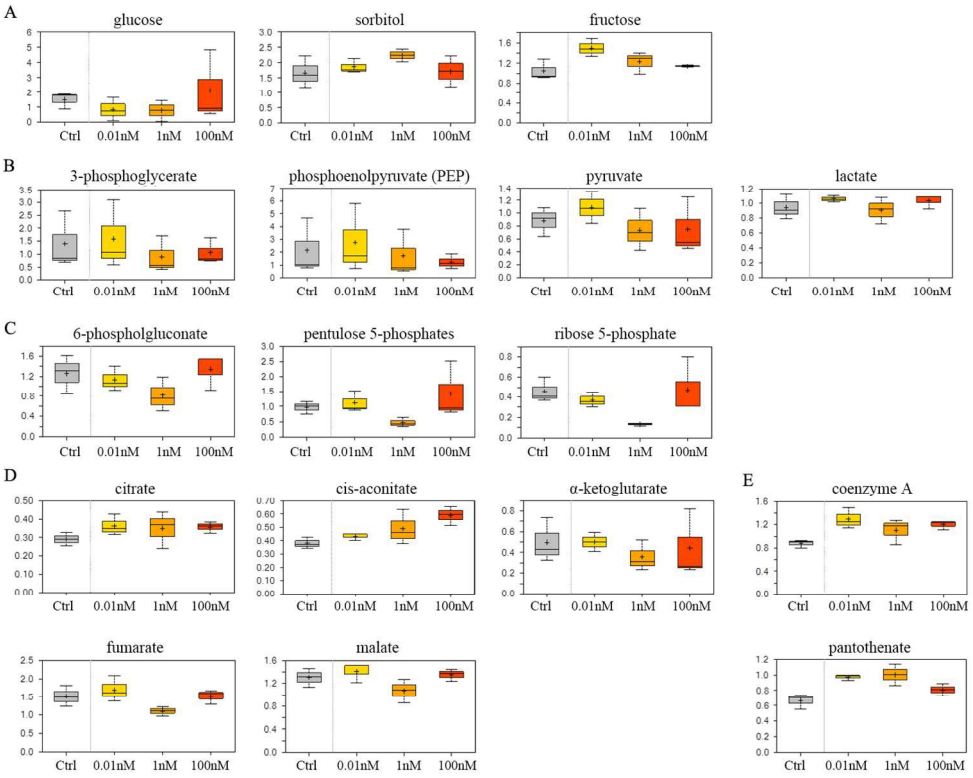


Fig 4
131x106mm (300 x 300 DPI)

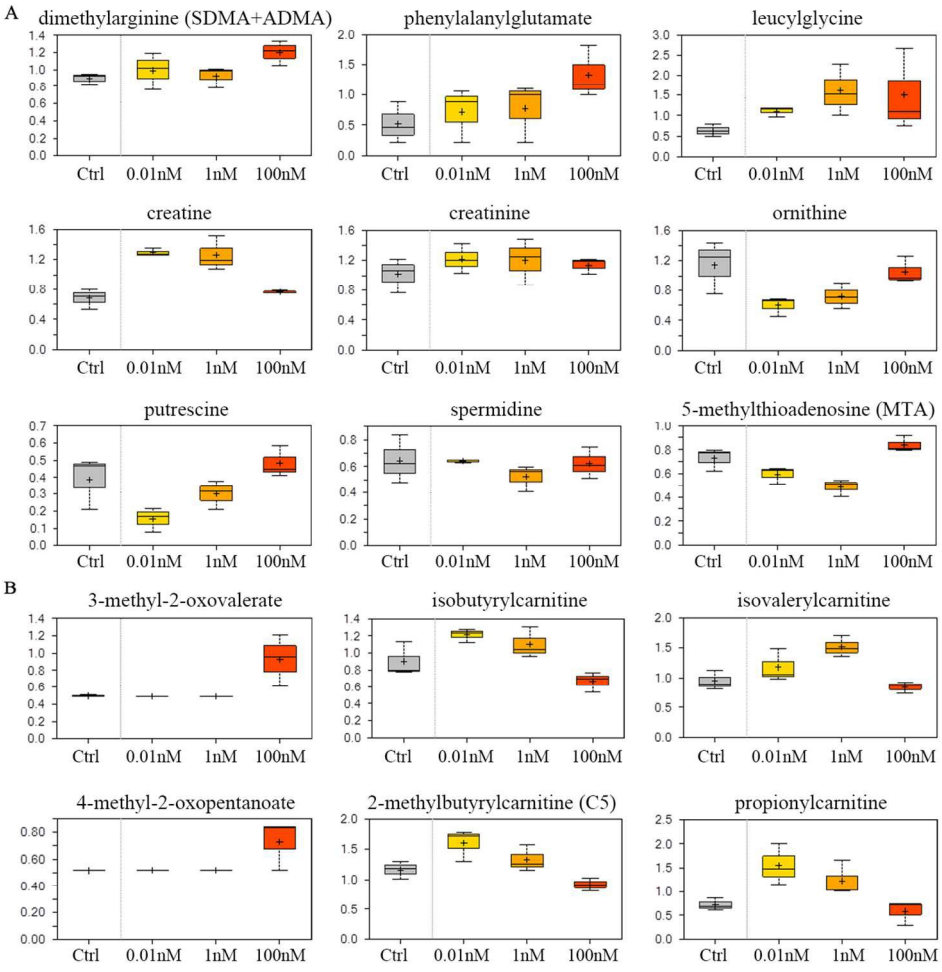


Figure 5
119x119mm (300 x 300 DPI)

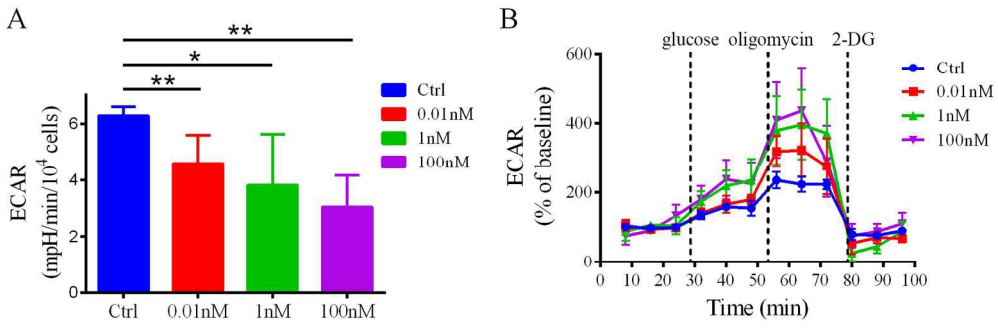


Fig 6
170x65mm (300 x 300 DPI)